Dalton Transactions

Dynamic Article Links

Cite this: *Dalton Trans.*, 2012, **41**, 7218

www.rsc.org/dalton

PAPER

Looking for the origin of the switch between coordination-captured helicates and catenates†

Lilit Aboshyan-Sorgho,[a] Martine Cantuel,[a] Gérald Bernardinelli[b] and Claude Piguet*[a]

Received 21st February 2012, Accepted 16th April 2012
DOI: 10.1039/c2dt30414g

Self-assembly of the linear segmental ligand **L5**, consisting of a tridentate binding unit flanked with two bidentate binding units, with a mixture of Fe^{II}/Ag^{I} yields the trinuclear coordination-captured [2]catenate $[AgFeAg(\mathbf{L5})_2]^{4+}$ instead of the planned isomeric double-stranded helicate. Replacing the octahedral (Fe^{II}) and tetrahedral (Ag^{I}) cations with Zn^{II}, which is compatible with both geometries, gives intricate mixtures of homometallic complexes upon reaction with the twin ligand **L6**, from which the macrocyclic dinuclear complex $[Zn_2(\mathbf{L6})]^{4+}$ can be isolated. Application of the thermodynamic site binding model attributes the origin of the ligand preference for producing single-stranded macrocycles, the precursors of the trinuclear catenate, to the abnormally low value of the effective molarity controlling the intramolecular connection leading to the usual double-stranded helical isomer.

Introduction

Taking advantage of the concept of coordination algorithms,[1] which implies that the stereoelectronic information stored in the ligands can be rationally deciphered by the preferences of the metal ions, Constable and coworkers were the first to exploit a sequence of bidentate and tridentate binding sites for the selective formation of a dimetallic helicate (HH)-$[CoAg(\mathbf{L1})_2]^{3+}$. In this dinuclear complex, the six-coordinate Co^{II} cation occupies the pseudo-octahedral site produced by two terpyridine units, whereas Ag^{I} lies in the remaining pseudo-tetrahedral site formed by the bipyridine units (Scheme 1).[2] Four years later, an extended series of closely related ligands **L2–L4** possessing various sequences of bidentate and tridentate segments were prepared by Smith and Lehn, and their complexation with mixtures of Cu(I)/Cu(II) or Cu^{I}/Fe^{II} cations led to the preparation of engineered trinuclear dimetallic double-stranded helicates with a predefined series of metal ions along the helical axis.[3] Between these two landmarks, Piguet and coworkers introduced a novel generation of segmental ligands, in which the standard six-membered aromatic pyridine rings used in **L1–L4** alternate with extended five-membered benzimidazole rings as exemplified in **L5** and **L6**.[4] Surprisingly, the reaction of the bidentate–tridentate–bidentate ligand **L5** with Fe^{II}, coded for octahedral coordination, and Ag^{I}, coded for tetrahedral coordination, did not yield the planned double-stranded dimetallic D_2-symmetrical helicate $[AgFeAg(\mathbf{L5})_2]^{4+}$ (Fig. 1 left, Constable's strategy),[5] but a diastereomeric mixture of the isomeric coordination-captured [2]catenates possessing two entwined metallamacrocycles with P or M helicities (Fig. 1 right).[6]

A thorough investigation of this trinuclear complex in solution eventually concluded that the three diastereomeric PP, MM and PM-$[AgFeAg(\mathbf{L5})_2]^{4+}$ catenates rapidly exchange on the NMR time scale at room temperature in acetonitrile, but their entangled structure is retained with no trace of helicates.[6] Though no satisfying rationalization could be proposed at that time for the thermodynamically preferred formation of coordination-captured [2]catenates over helicates in $[AgFeAg(\mathbf{L5})_2]^{4+}$,[7] Sauvage, Fujita and coworkers remarkably extended this approach for the preparation of self-assembled dimetallic $[((en)Pd)Cu(Pd(en))(\mathbf{L7})_2]^{5+}$ (en = 1,2-ethylenediamine)[8] and trimetallic $[RuCuM(\mathbf{L8})_2]^{5+}$ (M = Fe, Co, Cu, Zn)[9] metal-containing [2]catenates. Whereas the preference for catenate formation in the two latter cases was assigned to the well-established $[Cu^{I}(phenanthroline)_2]$ templating effect reinforced by some kinetic barriers induced by the use of inert Pd^{II} or Ru^{II} metals, the thermodynamic conditions required for the formation of a single topological isomer (helicate or catenate) remained elusive. A serendipitous approach using the closely related segmental ligand **L9** recently confirmed this delicate balance since the planned trinuclear double-stranded helicates $[AgFeAg(\mathbf{L9})_2]^{4+}$ (Constable's strategy) was the only complex formed upon reaction with octahedral Fe^{II} and tetrahedral Ag^{I},[10] whereas reaction with Hg^{II}, which displays no stereochemical preference and therefore may adopt both geometries, provided $[Hg_3(\mathbf{L9})_2]^{6+}$ as mixture of helicates and cyclometallated [2]catenates (Piguet's strategy).[11] The stepwise improvements of the thermodynamic modelling of metal-driven self-assembly processes (equilibrium 1) gained during the last decade eventually led to the emergence of the extended site binding model (eqn (2)), in which five 'easily' interpretable

[a]*Department of Inorganic and Analytical Chemistry, University of Geneva, 30 quai E. Ansermet, CH-1211 Geneva 4, Switzerland. E-mail: Claude.Piguet@unige.ch*
[b]*Laboratory of X-ray Crystallography, University of Geneva, 24 quai E. Ansermet, CH-1211 Geneva 4, Switzerland*

†Electronic supplementary information (ESI) available. CCDC 865559. For ESI and crystallographic data in CIF or other electronic format see DOI: 10.1039/c2dt30414g

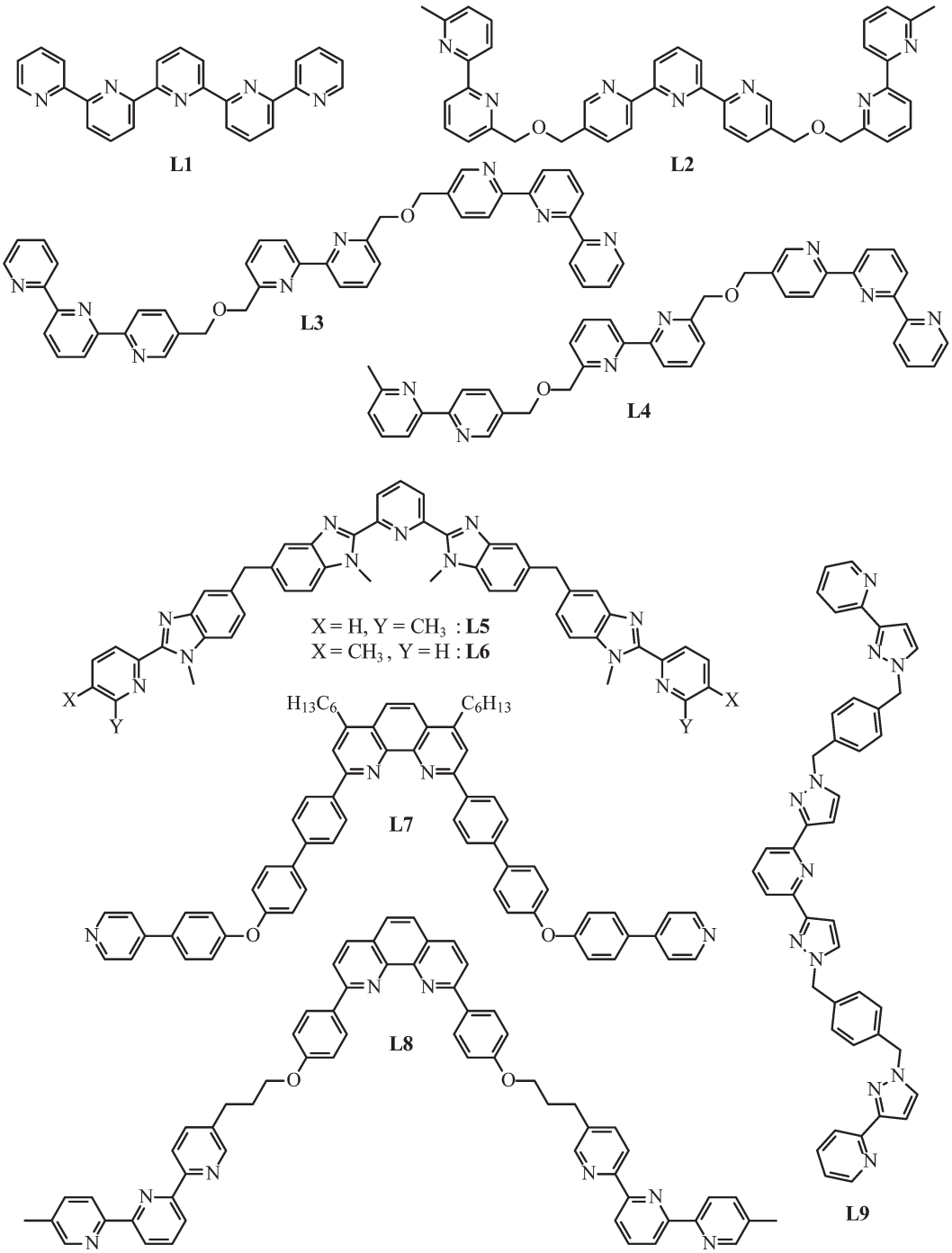

Scheme 1 Chemical structures of ligands **L1–L9**.

thermodynamic describers are now at hand for catching the pertinent driving forces responsible for the formation of specific metallosupramolecular architectures.[12]

$$n\mathbf{L} + m\mathrm{M} \rightleftharpoons [\mathrm{M}_m(\mathbf{L})_n]\ \beta_{m,n}^{\mathrm{M,L}} \quad (1)$$

$$\beta_{m,n}^{\mathrm{M,L}} = \mathrm{e}^{-(\Delta G_{m,n}^{\mathrm{M,L}}/RT)} = \omega_{m,n}^{\mathrm{chiral}}\omega_{m,n}^{\mathrm{M,L}}\prod_{i=1}^{mn} f_i^{\mathrm{M,L}}\prod_{i=1}^{mn-m-n+1} c_i^{\mathrm{eff}}\prod_{i<j}\mathrm{e}^{-\Delta E_{i,j}^{\mathrm{M,M}}/RT}\prod_{k<l}\mathrm{e}^{-\Delta E_{k,l}^{\mathrm{L,L}}/RT} \quad (2)$$

Taking advantage of this simple rationalization, we reconsider here the conditions and the origin of the selective formation of catenates *versus* helicates with the segmental ligands **L5–L6**.

Results and discussion

Theoretical model and strategy

Using the van't Hoff equation with a standard concentration for the reference state of c^{θ} = 1 M,[13] the extended site

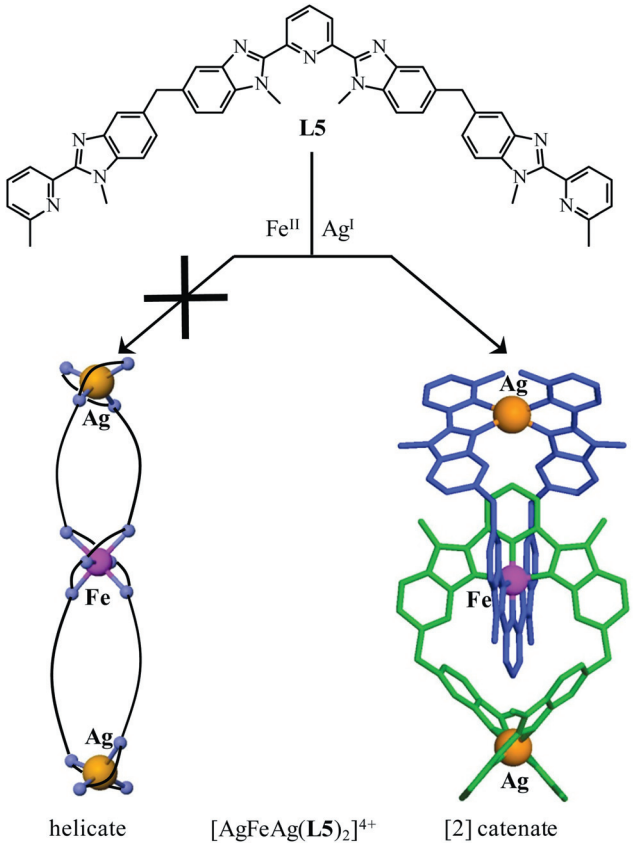

Fig. 1 Self-assembly of the trinuclear dimetallic $[AgFeAg(\mathbf{L5})_2]^{4+}$ cation showing the planned (non-observed) helicate topology (left) and the observed [2]catenate structure. The crystal structure of the *meso*-catenate PM-$[AgFeAg(\mathbf{L5})_2]^{4+}$ is shown.[6]

binding model transforms the thermodynamic formation constant $\beta_{m,n}^{M,L}$ of any metal-containing self-assembly processes into a sum of free energy changes (eqn (2)). The first contribution $\Delta G_1^{M,L} = -RT\ln(\omega_{m,n}^{chiral}\omega_{m,n}^{M,L})$ corresponds to the changes in rotational entropy occurring when the reactants are transformed into products. It can be computed by using the symmetry numbers (σ^{ext}, σ^{int} and σ^{chiral}) controlling the statistical factors of the assembly $\omega_{m,n}^{chiral}\omega_{m,n}^{M,L}$ as soon as the point groups of the various partners are at hand.[14] Applied to the formation of $[AgFeAg(\mathbf{L}\boldsymbol{k})_2]^{4+}$ (k = 5, 6) in equilibrium 3, we calculate $\omega_{1,2,2}^{chiral}\omega_{1,2,2}^{Fe,Ag,\mathbf{L}\boldsymbol{k}} = 6912$ for both [2]catenate and helicate topologies (eqn (4) and (5), Fig. S1, ESI†).

$$2\mathbf{L}\boldsymbol{k} + [Fe(CH_3CN)_6]^{2+} + 2[Ag(CH_3CN)_4]^{+} \rightleftharpoons [AgFeAg(\mathbf{L}\boldsymbol{k})_2]^{4+} + 14CH_3CN\ \beta_{1,2,2}^{Fe,Ag,\mathbf{L}\boldsymbol{k}} \quad (3)$$

The second term $\Delta G_2^{M,L} = -RT\sum_i f_i^{M,L}$ represents the intermolecular metal–ligand binding processes, including desolvation, which is partitioned between the intrinsic affinity of the central tridentate binding site for Fe(II) (f_{tri}^{Fe}) and the intrinsic affinity of Ag(I) for the terminal binding sites (f_{bi}^{Ag}).[15] Again, the whole contribution $(f_{tri}^{Fe})^2(f_{bi}^{Ag})^4$ to the cumulative formation constants is similar for both helicate and [2]catenate complexes (eqn. (4) and (5)).

$$\beta_{1,2,2}^{Fe,Ag,\mathbf{L}\boldsymbol{k}}(\text{helicate}) = 6912(f_{tri}^{Fe})^2(f_{bi}^{Ag})^4(EM_{helicate})^2 \times (u_{helicate}^{Fe,Ag})^2 u_{tri}^{\mathbf{L}\boldsymbol{k},\mathbf{L}\boldsymbol{k}}(u_{bi}^{\mathbf{L}\boldsymbol{k},\mathbf{L}\boldsymbol{k}})^2 \quad (4)$$

$$\beta_{1,2,2}^{Fe,Ag,\mathbf{L}\boldsymbol{k}}(\text{catenate}) = 6912(f_{tri}^{Fe})^2(f_{bi}^{Ag})^4(EM_{catenate})^2 \times (u_{catenate}^{Fe,Ag})^2 u_{tri}^{\mathbf{L}\boldsymbol{k},\mathbf{L}\boldsymbol{k}}(u_{bi}^{\mathbf{L}\boldsymbol{k},\mathbf{L}\boldsymbol{k}})^2 \quad (5)$$

Among the six metal–ligand binding connections occurring in $[AgFeAg(\mathbf{L}\boldsymbol{k})_2]^{4+}$,[16] four are intermolecular and depend on the probability of the association of two partners freely moving and statistically dispersed in the condensed phase. However, the two remaining metal–ligand coordination events leading, for instance, to the formation of the terminal pseudo-tetrahedral $[Ag^I(bzimpy)_2]$ (bzimpy = benzimidazol-2-yl-pyridine) entities in $[AgFeAg(\mathbf{L}\boldsymbol{k})_2]^{4+}$ are intramolecular. Their efficiency depends on the effective concentrations (c^{eff}) of the connected interacting partners imposed by the reduced motion of the ligand strands.[17] Both enthalpic and entropic contributions to c^{eff} must be carefully considered, but reliable theoretical predictions are difficult.[18] We therefore rely here on the concept of experimental effective molarity (EM), which empirically transforms the intermolecular Ag-bzimpy affinity f_{bi}^{Ag} into its intramolecular counterpart $f_{bi}^{Ag}(\text{intra}) = EM f_{bi}^{Ag}$.[12,17] Since the length of the atomic chains connecting the two units undergoing intramolecular macrocyclization are similar for both catenate and helicate topologies (20 atoms), the entropic part of EM can be reasonably taken as similar (Fig. 1 and Fig. S2, ESI†).[18] However, the completely different structures adopted by the crooked polyatomic connectors involve different enthalpic contributions, and specific effective molarities must be used for the helicate (eqn (4)) and for the catenate (eqn (5)). Finally, the homocomponent interaction produced by the close location of two metals connected to the same ligand ($u^{Fe,Ag} = e^{-\Delta E^{Fe,Ag}/RT}$) may significantly contribute to the overall stability, while the related correction for two binding units coordinated to the same metal ($u_{bi}^{\mathbf{L}\boldsymbol{k},\mathbf{L}\boldsymbol{k}} = e^{-\Delta E_{bi}^{\mathbf{L}\boldsymbol{k},\mathbf{L}\boldsymbol{k}}/RT}$ and $u_{tri}^{\mathbf{L}\boldsymbol{k},\mathbf{L}\boldsymbol{k}} = e^{-\Delta E_{tri}^{\mathbf{L}\boldsymbol{k},\mathbf{L}\boldsymbol{k}}/RT}$) can be safely neglected for the self-assemblies of charged complexes in polar solvents.[12d,19,20] The ratio of the incriminated formation constants modelled in eqn (4) and (5) gives eqn (6), from which we conclude that the change in effective molarities between the helicate and [2]catenate is crucial for stabilizing one specific topology.

$$\frac{\beta_{1,2,2}^{Fe,Ag,\mathbf{L}\boldsymbol{k}}(\text{helicate})}{\beta_{1,2,2}^{Fe,Ag,\mathbf{L}\boldsymbol{k}}(\text{catenate})} \approx \left(\frac{EM_{helicate}}{EM_{catenate}}\right)^2 \quad (6)$$

Whereas a few experimental EM values have been reported for helicates with d- or f-block cations (Fig. 2),[20,21] estimations of effective molarities for alternative catenate structures are lacking. In order to build some rational bases for the preferred formation of the trinuclear catenate with **L5** (Fig. 1), we have established a simple protocol for a preliminary investigation. Firstly, ligand **L5** is replaced with **L6**, in which the solubilizing methyl groups bound to the terminal pyridine rings are shifted away from the coordinating nitrogen atoms, thus minimizing interligand interactions, a necessary condition for neglecting $u_{bi}^{\mathbf{L}\boldsymbol{k},\mathbf{L}\boldsymbol{k}} = e^{-\Delta E_{bi}^{\mathbf{L}\boldsymbol{k},\mathbf{L}\boldsymbol{k}}/RT}$ in eqn (4) and (5). Secondly, we plan to

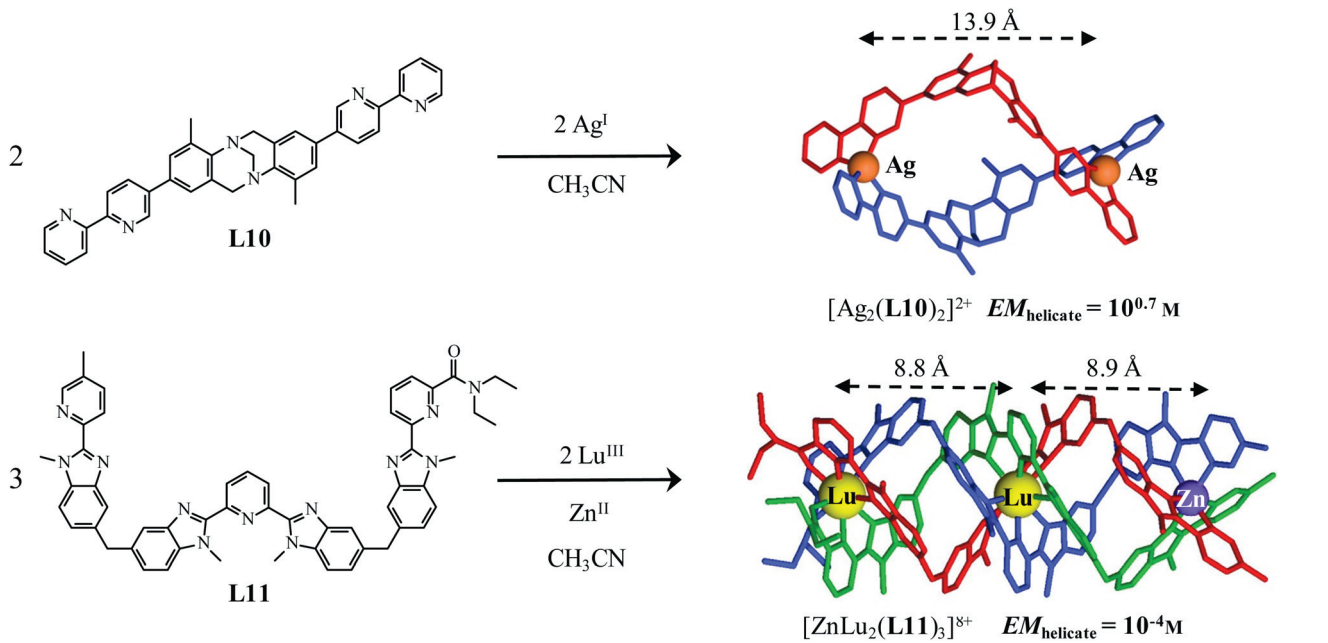

Fig. 2 Self-assembly of helicates for which the experimental effective molarities were determined. Formation of (a) the dinuclear macrocyclic double-stranded helicate $[Ag_2(\mathbf{L10})_2]^{2+}$,[20] and (b) the trinuclear macrotetracyclic triple-stranded helicate $[ZnLu_2(\mathbf{L11})_3]^{8+}$.[21]

restrict the exploration of the energy hypersurface of the assembly to only two partners, the segmental ligand **L6** and a single type of metal ion, Zn^{II}, which displays no stereochemical preference (d^{10} electronic configuration) and can thus adopt both pseudo-tetrahedral or pseudo-octahedral geometries.

Following the self-assembly of L6 with Zn(II) in solution

ESI-MS titrations of **L6** (2×10^{-4} M) with $Zn(CF_3SO_3)_2$ in acetonitrile show the preferred formation of $[Zn(\mathbf{L6})_2]^{2+}$ for all stoichiometric ratios, together with traces of $[Zn(\mathbf{L6})_3]^{3+}$ in default of metal, and no negligible quantities of $[Zn_2(\mathbf{L6})_2]^{4+}$ in excess of metal (detected as its gas-phase triflate adducts, Fig. 3). None of these species are of straightforward interest for catching parameters pertinent for the competitive formation of trinuclear helicates *versus* catenates with **L6**. Parallel spectrophotometric titrations of **L6** recorded at the same concentration, but in $CHCl_3$–CH_3CN (1 : 1), show a complicated variation of the ligand-centered absorption spectra (Fig. 4a) with an expected marked end point for Zn : **L6** = 0.5, together with smoother, but non-negligible inflexions for Zn : **L6** = 1.0, 1.5 and 2.0 (Fig. 4b). Factor analysis[22] suggests the formation of at least five absorbing species (*i.e.* **L6** and four complexes), but we were unable to fit the spectrophotometric data to any reasonable set of thermodynamic equilibria involving mono- and polynuclear Zn^{II} complexes. ^1H NMR titrations recorded at higher concentration do not clarify the situation with the observation of broad and unresolved spectra which are typical for the existence of intricate mixtures of complexes displaying intermediate exchange rates on the NMR time scale.

However, the addition of 1/3 equivalent of $La(CF_3SO_3)_3 \cdot 3H_2O$ to **L6**, prior to titration with Zn^{II} is known to simplify the assembly process, with the emergence of the linear dimetallic

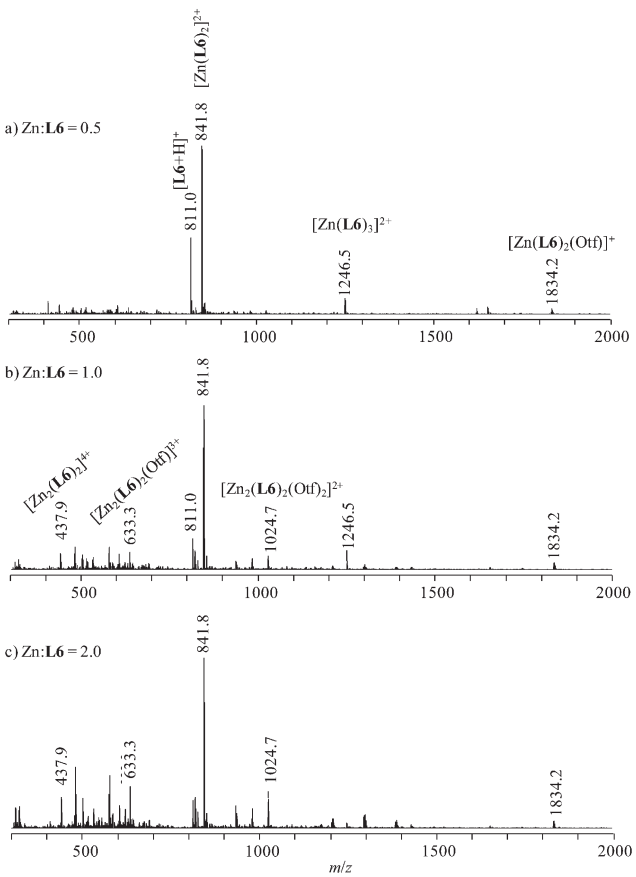

Fig. 3 ESI-MS titrations of **L6** (2×10^{-4} M) with $Zn(CF_3SO_3)_2$ for (a) Zn : **L6** = 0.5, (b) Zn : **L6** = 1.0 and (c) Zn : **L6** = 2.0 (CH_3CN, 298 K; $Otf^- = CF_3SO_3^-$).

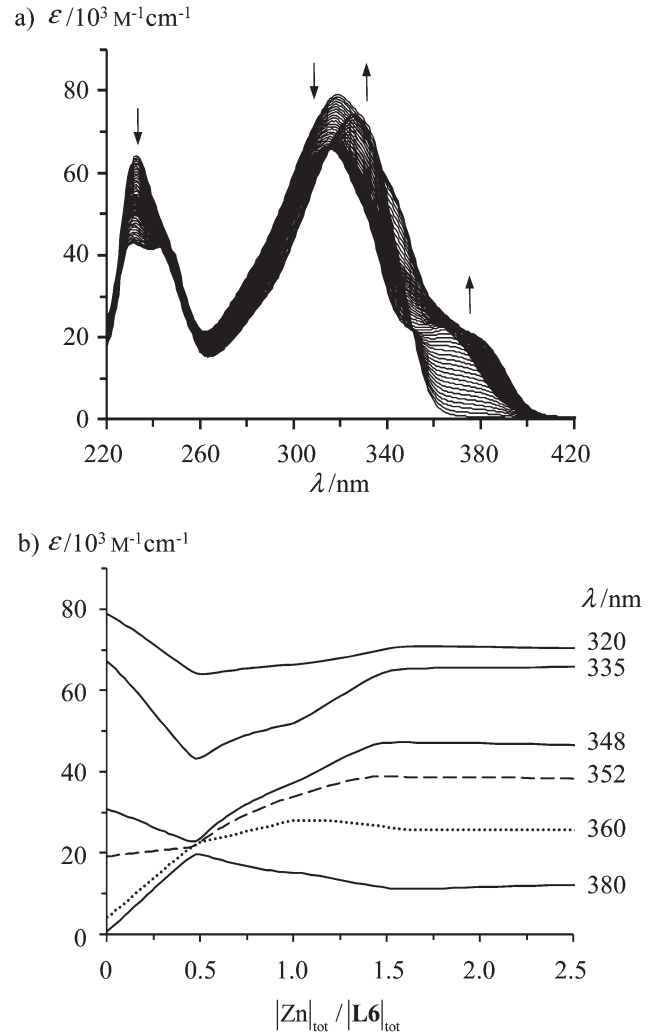

Fig. 4 Variation of (a) absorption spectra and (b) corresponding variation of molar extinctions at six different wavelengths observed for the spectrophotometric titrations of **L6** (2×10^{-4} M) with $Zn(CF_3SO_3)_2$ ($CHCl_3$–CH_3CN (1 : 1), 298 K).

triple-stranded helicates $[LaZn_n(\mathbf{L6})_3]^{(3+2n)+}$ (n = 1, 2) as the major species in the mixture at ten millimolar concentrations (Fig. S3, ESI†).[24]

Due to the efficient solvation of the polyaromatic ligand by chloroform,[23] the stability of the saturated triple-stranded helicate $[LaZn_2(\mathbf{L6})_3]^{7+}$ is limited in $CHCl_3$–CH_3CN solutions and considerable numbers of homometallic complexes coexist in solution at submillimolar concentrations, among which $[Zn(\mathbf{L6})_2]^{2+}$ and $[Zn_2(\mathbf{L6})_2]^{4+}$ can be identified (Fig. S4a, ESI†).[24] Interestingly, the introduction of smaller lanthanide cations is prone to further destabilize the triple-helical edifices,[25] and the stepwise replacement of the largest Ln = La(III) cation (nine-coordinate ionic radius $R_{La}^{CN=9}$ = 1.216 Å) with Ln = Eu(III) ($R_{Eu}^{CN=9}$ = 1.120 Å) and Ln = Yb(III) ($R_{Yb}^{CN=9}$ = 1.042 Å) in $[LnZn_2(\mathbf{L6})_3]^{7+}$ indeed favors dissociation with the concomitant formation of increasing amounts of $[Zn(\mathbf{L6})_2]^{2+}$, $[Zn_2(\mathbf{L6})_2]^{4+}$ together with traces of a novel species with a Zn : **L6** = 2.0 ratio detected by ESI-MS as $[Zn_2(\mathbf{L6})(CF_3SO_3)_2]^{2+}$ at m/z = 618.5 (Fig. S4b,c, ESI†). The latter unsaturated dinuclear $[Zn_2(\mathbf{L6})]^{4+}$ complex is an attractive candidate for addressing helicate/catenate competition with **L6** (*vide infra*), and its concentration in solution can be optimized by adding moderately coordinating chloride counter-anions in pure acetonitrile to give $[Zn_2(\mathbf{L6})Cl(CF_3SO_3)]^{2+}$ at m/z = 562.1, in which the zinc coordination spheres are completed without removing **L6** (Fig. 5).

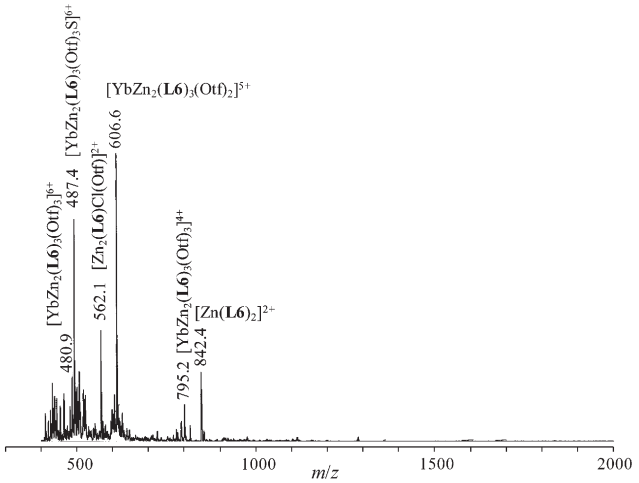

Fig. 5 ESI-MS spectrum of $[YbZn_2(\mathbf{L6})_3]^{7+}$ with added chloride anions (5×10^{-4} M, CH_3CN, 298 K, $Otf^- = CF_3SO_3^-$).

Isolation, crystal and molecular structures of $[Zn_2(L6)Cl(H_2O)_2(CF_3SO_3)](CF_3SO_3)_2$

Diffusion of diethylether into a concentrated aqueous acetonitrile solution containing **L6** (1 eq.), $Zn(CF_3SO_3)_2$ (2 eq.) and NaCl (1 eq.) gave 75% yield of $[Zn_2(\mathbf{L6})Cl](CF_3SO_3)_3{\cdot}2H_2O{\cdot}2.5CH_2Cl_2$ as a white microcrystalline powder. Transparent prisms of $[Zn_2(\mathbf{L6})Cl](CF_3SO_3)_3{\cdot}2H_2O{\cdot}4CH_3CN$ (**1**) suitable for X-ray diffraction studies were obtained by recrystallization from acetonitrile–diethylether. The crystal structure of **1** (Table S1, ESI†) shows it to be composed of a single-stranded macrocyclic $[Zn_2(\mathbf{L6})Cl(CF_3SO_3)(H_2O)_2]^{2+}$ cation (Fig. 6), two non-coordinated triflate anions hydrogen-bound to the coordinated water molecules (Fig. S5 and Table S2, ESI†), and four interstitial acetonitrile molecules. The ligand strand is twisted about a helical axis perpendicular to the pseudo-twofold axis passing through the Zn atoms, leading to a linear progression of 6.77 Å for a complete turn (*i.e.* pitch = 6.77 Å, Fig. 7a). All Zn–N and Zn–O(water) bond distances are standard (Table S3, ESI†),[26] while the Zn–O(triflate) bond length of 2.340(7) Å is longer because of the poorly coordinating character of this counter-anion. Zn1 is five-coordinated by the central tridentate binding unit, one oxygen of a water molecule and a chloride anion. The pyridine nitrogen atom N1, O1w and Cl1 form the triangular basis of a distorted trigonal bipyramid (in-plane bonding angles in the range 108–134° instead of 120° for an ideal trigonal bipyramid with Zn1 located at 0.020(3) Å above this plane in the direction of N7), whereas N2 and N7 occupy the axial positions (∠ N2–Zn1–N7 = 150.2(2)° instead of 180° in an ideal trigonal bipyramid, Fig. 6).

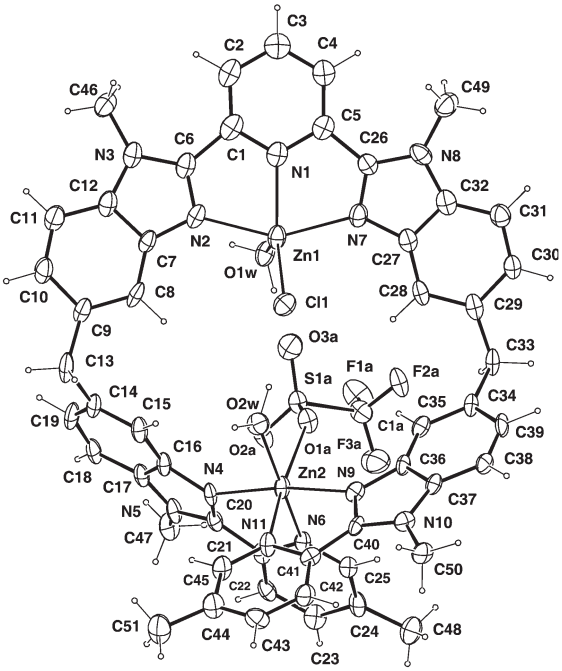

Fig. 6 ORTEP perspective view of the cation $[Zn_2(\mathbf{L6})Cl(CF_3SO_3)(H_2O)_2]^{2+}$ perpendicular to the pseudo-twofold axis passing through the Zn atoms with numbering scheme. Ellipsoids are represented at the 40% probability level.

The metal ionic radius computed by using Shannon's definition[27] with r_N = 1.46 Å, r_O = 1.35 Å and r_{Cl} = 1.81 Å amounts to $R_{Zn1}^{CN=5}$ = 0.62 Å, a value slightly smaller than the 0.68 Å expected for five-coordinated Zn^{II}, but in line with the efficient coordination of this cation to the tridentate binding unit of the ligand. The second zinc atom, Zn2, is pseudo-octahedrally coordinated by the two terminal bidentate binding units of the ligand strand, while the two *cis* remaining sites are occupied by a water molecule and a monodentate triflate anion. The main distortions from a perfect octahedron result from the constrained chelate bite angles imposed by the bidentate aromatic binding units (N4–Zn_2–N6 = 78.4(2)°, N9–Zn_2–N11 = 77.5(3)° Table S3, ESI†). The calculated metal ionic radius $R_{Zn2}^{CN=6}$ = 0.72 Å is close to the 0.74 Å expected for six-coordinated Zn(II) cations.[27]

Interestingly, the two metal atoms in $[Zn_2(\mathbf{L6})Cl(CF_3SO_3)(H_2O)_2]^{2+}$ are only bridged by the helical ligand strand, a situation similarly encountered for the [2]catenate cation $[AgFeAg(\mathbf{L5})_2]^{4+}$ (Fig. 7b).[6] Except for a shorter intermetallic contact distance of Zn···Zn = 6.352(1) Å (Fe···Ag = 8.08–8.16 Å),[6] which can be reasonably assigned to the absence of the second entangled macrocyclic ring found in the catenate, the isolated cation $[Zn_2(\mathbf{L6})Cl(CF_3SO_3)(H_2O)_2]^{2+}$ satisfyingly mimics the preliminary intramolecular macrocyclization process responsible for the formation of catenates instead of helicates with **L5** and **L6** (Fig. 7b). We cannot however completely exclude some minor stabilizing contributions from intermolecular π-stacking interactions, which play a part in the overall packing in the crystalline state (Fig. S6 and Table S4, ESI†).

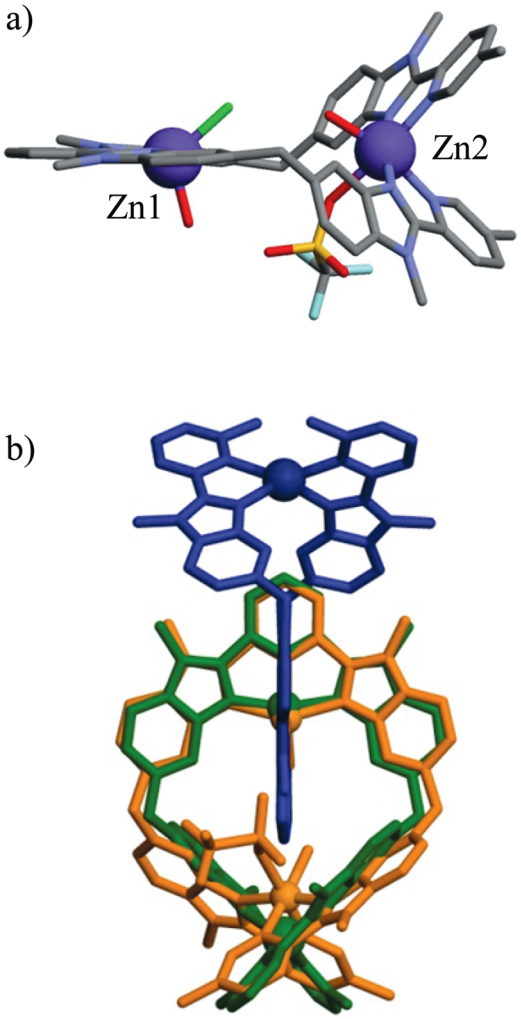

Fig. 7 Views of the molecular structure of the cation $[Zn_2(\mathbf{L6})Cl(CF_3SO_3)(H_2O)_2]^{2+}$ (a) perpendicular to the pseudo-twofold axis passing through the two Zn atoms and to the helical axis (color code: C = grey, N = dark blue, O = red, S = yellow, F = light blue, Zn = violet) and (b) along the helical axis (color code: orange) superimposed with the molecular structure of the [2]catenate complex $[AgFeAg(\mathbf{L5})_2]^{4+}$ (color code: green and blue).

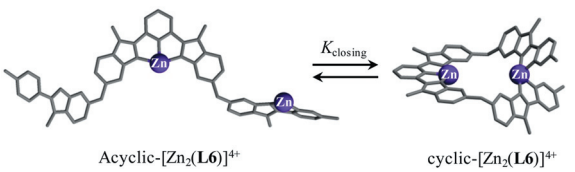

Fig. 8 Equilibrium (7) modelling the macrocyclization process responsible for the formation of the single-stranded macrocyclic $[Zn_2(\mathbf{L6})]^{2+}$ complex.

The exclusive isolation of $[Zn_2(\mathbf{L6})]^{4+}$ as a metallomacrocycle instead of its non-cyclic counterpart in equilibrium (7) agrees with the well-respected principle of maximum site occupancy (Fig. 8),[28] which implies that the effective molarity for this intramolecular connection, $EM_{closing}$, is large enough for not overcoming the driving force provided by the complexation of

Zn(II) to the second terminal bidentate binding unit (*i.e.* $EM_{closing} f_{bi}^{Zn} > 1$ in eqn (8)).

$$K_{closing} = \omega_{closing} EM_{closing} f_{bi}^{Zn} u_{bi}^{L6,L6} \approx EM_{closing} f_{bi}^{Zn} \quad (8)$$

Since the statistical factor $\omega_{closing} = 1$ (Fig. S7, ESI†) and the interligand interaction u_{bi}^{L7} can be reasonably neglected,[19,20] the exclusive detection of the macrocyclic complex $[Zn_2(\mathbf{L6})]^{2+}$ is associated with $K_{closing} \geq 10$, which translates into $EM_{catenate} \equiv EM_{closing} \geq 10/f_{bi}^{Zn}$ (eqn (8)), where $EM_{closing}$ corresponds to the average correcting term for intramolecular connections occurring in the final catenate. Taking $f_{bi}^{Zn} \approx 10^6$ found for $[ZnLu_2(\mathbf{L11})_3]^{8+}$ in CH_3CN[19] eventually gives $EM_{catenate} \geq 10^{-5}$ M in this solvent, a value which represents the necessary condition for a 90% switching from a non-cyclic complexation process (Fig. 8 left, considered as the precursor step for linear helicates), toward macrocyclization (Fig. 8 right, the precursor step for the formation of [2]catenates).

A concomitant estimation of $EM_{catenate}$ can be obtained from the ^{1}H NMR spectrum of $[Zn_2(\mathbf{L6})Cl(CF_3SO_3)(H_2O)_2]^{2+}$ (2.5 mM in acetonitrile, Fig. 9), which indeed shows the coexistence of $[Zn_2(\mathbf{L6})]^{4+}$ (72% of the ligand speciation) with equal amounts of $[Zn(\mathbf{L6})_2]^{2+}$ and $[Zn_3(\mathbf{L6})_2]^{6+}$, each counting for 14% of the ligand speciation (eqn (9); Appendix 1, ESI†).[29]

$$4[Zn_2(\mathbf{L6})]^{4+} \rightleftharpoons [Zn(\mathbf{L6})_2]^{2+} + [Zn_3(\mathbf{L6})_2]^{6+} + 4Zn^{2+} \quad K_{exch} \quad (9)$$

The two minor complexes are easily identified through their abnormally shielded signals of equal intensities at 5.96 ppm and 5.89 ppm (Fig. 9), which are diagnostic for the formation of pseudo-octahedral [Zn(bis(benzimidazol-2-yl)pyridine)] units, in which H8 lies in the aromatic shielding cone of the second tridentate binding unit, as previously established for $[Fe(\mathbf{L6})_2]^{2+}$ (5.53 ppm) and $[FeAg_2(\mathbf{L6})_2]^{4+}$ (5.24 ppm).[5] On the other hand, the single-stranded $[Zn_2(\mathbf{L6})]^{4+}$ complex obviously does not undergo interstrand anisotropic shielding effects, and the eleven signals of its aromatic protons lie in the usual 7.50–8.50 ppm range (Fig. 9, assignment *via* $\{^1H–^1H\}$-COSY and $\{^1H–^1H\}$-NOESY spectroscopies). Diffusion Ordered SpectroscopY (DOSY-NMR, CD3CN, 298 K) further supports eqn (9) with almost identical auto-diffusion coefficients for $[Zn(\mathbf{L6})_2]^{2+}$ ($D_{ZnL2} = 1.41(4) \times 10^{-9}$ m^2 s^{-1}) and $[Zn_3(\mathbf{L6})_2]^{4+}$ ($D_{Zn3L2} = 1.37(4) \times 10^{-9}$ m^2 s^{-1}) which possess two ligand strands, whereas the lighter $[Zn_2(\mathbf{L6})]^{4+}$ complex is more mobile ($D_{Zn2L} = 1.62(3) \times 10^{-9}$ m^2 s^{-1}).[30] The integration of the signals found for H8 in the three complexes allows the complete speciation, from which $K_{exch} = 8.2 \times 10^{-10}$ is obtained (Appendix 1, ESI†). Interestingly, K_{exch} can be modelled with the extended site binding model (eqn (10), Appendix 2, ESI†), and comparison with its experimental value eventually gives eqn (11) after introducing $f_{bi}^{Zn} \approx 10^6$, the adequate statistical factor $\omega_{exch} = 1/2\,654\,208$ and the reasonable approximation $u_{bi}^{L6} \approx u_{tri}^{L6}$.[19]

$$K_{exch} = \omega_{exch} \left(\frac{u_{tri}^{L6,L6}}{u_{bi}^{L6,L6}} \frac{1}{EM_{catenate} (f_{bi}^{Zn})^2 u^{Zn,Zn}} \right)^2 \quad (10)$$

$$EM_{catenate} = \frac{1}{u^{Zn,Zn} (f_{bi}^{Zn})^2} \sqrt{\frac{\omega_{exch}}{K_{exch}}} = \frac{2.15 \times 10^{-11}}{u^{Zn,Zn}} \quad (11)$$

The exact value of the intramolecular intermetallic interaction $u^{Zn,Zn} = \exp(-\Delta E^{Zn,Zn}/RT)$ is crucial for calculating the effective molarity, but no experimental value is available for the two Zn^{2+} separated by approximately 6–8 Å in complexes $[Zn_2(\mathbf{L6})]^{4+}$ and $[Zn_3(\mathbf{L6})_2]^{6+}$ displaying rough ellipsoidal shapes.[19] Taking the larger repulsion $u^{M,M} = 10^{-6}$ reported for the double-stranded d-block helicates $[M_2(\mathbf{L10})_2]^{2+}$ (M = Cu, Ag) with single charged cations in acetonitrile as a minimum threshold for $u^{Zn,Zn}$ operating between two doubly-charged Zn^{2+} cations in $[Zn_2(\mathbf{L6})]^{4+}$,[20] we finally estimate $EM_{catenate} \geq 2 \times 10^{-5}$ M.

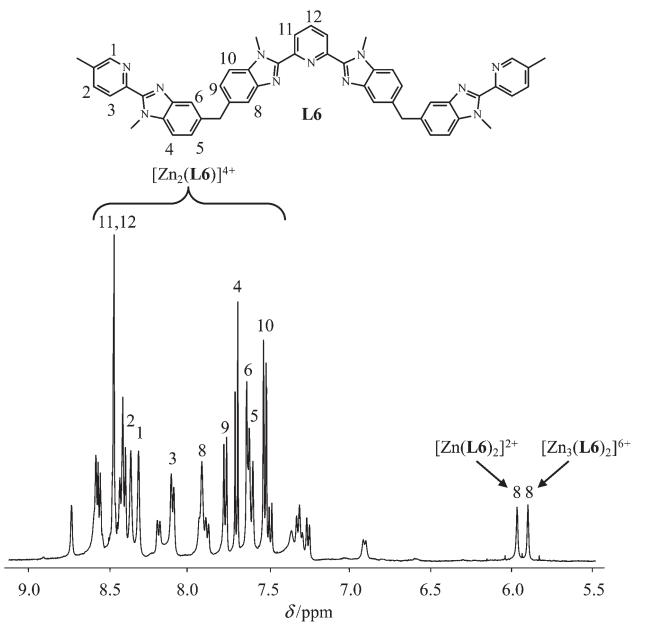

Fig. 9 Aromatic part of the ^{1}H NMR spectrum of $[Zn_2(\mathbf{L6})Cl(CF_3SO_3)(H_2O)_2](CF_3SO_3)_2$ with numbering scheme and partial assignment for $[Zn_2(\mathbf{L6})]^{4+}$, $[Zn(\mathbf{L6})_2]^{2+}$ and $[Zn_3(\mathbf{L6})_2]^{6+}$ (2.5 mM, CD_3CN, 293 K).

Conclusion

Both thermodynamic approaches (eqn (7) and (9)) converge to an effective molarity of $EM_{catenate} \geq 2 \times 10^{-5}$ m for the formation of the dinuclear macrocyclic precursor $[Zn_2(\mathbf{L6})]^{4+}$, a value which compares well with the $EM_{helicate}^{triple\text{-}stranded} = 10^{-4}$ m found for the formation of the triple-stranded helicate $[ZnLu_2(\mathbf{L11})_3]^{8+}$ using the closely related segmental ligand **L11** (Fig. 2).[19] This probably contributes to the complicated speciation observed for the reaction of **L6** with mixtures of Zn^{II}/La^{III} cations.[24] In absence of f-block metals, triple-stranded helicates cannot be formed and the [2]catenate $[M_3(\mathbf{L}k)_2]$ may only compete with the putative double-stranded helicates $[M_n(\mathbf{L}k)_2]$ (n = 2, 3) (Fig. 1). Since all spectroscopic data points to the quantitative formation of the [2]catenate isomer with no trace of helicate, eqn (6) can be re-written as

$$\frac{\beta_{1,2,2}^{M1,M2,\mathbf{L}k}(\text{helicate})}{\beta_{1,2,2}^{M1,M2,\mathbf{L}k}(\text{catenate})} \approx \left(\frac{EM_{helicate}^{double\text{-}stranded}}{EM_{catenate}} \right)^2 < 10^{-3} \quad (6')$$

Introducing $EM_{catenate} \geq 2 \times 10^{-5}$ M, we obtain $EM_{helicate}^{double\text{-}stranded} < EM_{catenate}/31.6 = 6 \times 10^{-7}$ M, a value which is more than two orders of magnitude smaller than the EM found for the formation of triple-stranded helicates with closely related segmental ligands. We conclude that, despite the fact that **L5** and **L6** have been originally designed to favor the formation of helicates with mixtures of d- and f-block metal ions,[5] the alternative [2]catenate isomer appears to be a fearsome competitor in absence of an f-block cation because of the abnormally large penalty brought by the intramolecular connection processes responsible for the formation of double-stranded helicates. Following the recent rational exploitation of the effective molarity for the selective preparation of unsaturated double-stranded precursors instead of the more common saturated triple-stranded products,[31] the preferred formation of trinuclear coordination-captured [2]catenates over double-stranded helicates further extends this approach and opens attractive perspectives for the design of sophisticated coordination-driven self-assembly processes according to both fundamental (*i.e.* understanding) and practical (*i.e.* profitable) points of view.

Experimental

Solvents and starting materials

These were purchased from Fluka AG or Aldrich and used without further purification unless otherwise stated. The ligand **L6** was prepared according to a literature procedure.[4] Acetonitrile was distilled over calcium hydride. The triflate salts Ln$(CF_3SO_3)_3 \cdot xH_2O$ (Ln = La, Eu, Yb; x = 2–4) were prepared from the corresponding oxides (99.99%) and dried according to published procedures.[32] The Ln content of solid salts was determined by complexometric titrations with Titriplex III (Merck) in the presence of urotropine and xylene orange.[33]

Preparation of the complex $[Zn_2(L6)Cl](CF_3SO_3)_3 \cdot 2H_2O \cdot 4CH_3CN$ (1)

A solution of $Zn(CF_3SO_3)_2$ (22.4 mg, 6.2×10^{-5} mol, 2 eq.) and NaCl (1.8 mg, 3.1×10^{-5} mol, 1 eq.) in 1% aqueous acetonitrile (4 cm^3) was added to a solution of **L6** (25 mg, 3.1×10^{-5} mol, 1 eq.) in dichloromethane (4 cm^3). After stirring for 12 h at 40 °C, the solution was filtered and diethylether was slowly diffused for 48 h. The resulting white microcrystalline powder was separated by filtration and dried to give 75% of $[Zn_2(\mathbf{L6})Cl](CF_3SO_3)_3 \cdot 2H_2O \cdot 2.5CH_2Cl_2$ (38.3 mg, 2.3×10^{-5} mol). Elemental analysis: calcd for $Zn_2C_{56.5}H_{52}N_{11}Cl_6O_{11}F_9S_3$ (MM = 1671.78) %C 40.60, %H 3.14, % N 9.22. Found %C 40.63, %H 3.09, %N 9.13. Slow recrystallization from acetonitrile–diethyl ether produced transparent prisms of $[Zn_2(\mathbf{L6})Cl](CF_3SO_3)_3 \cdot 2H_2O \cdot 4CH_3CN$ (**1**) suitable for X-ray diffraction studies.

Spectroscopic and analytical measurements

Spectrophotometric titrations were performed with a J&M diode array spectrometer (Tidas series) connected to an external computer. In a typical experiment, 50 cm^3 of ligand in acetonitrile (10^{-4} mol dm^{-3}) were titrated at 293 K with a solution of $Zn(CF_3SO_3)_2$ (10^{-3} mol dm^{-3}) in acetonitrile or acetonitrile : chloroform (1 : 1) under an inert atmosphere. After each addition of 0.20 cm^3, the absorbance was recorded using Hellma optrodes (optical path length 0.1 cm) immersed in the thermostated titration vessel and connected to the spectrometer. Mathematical treatment of the spectrophotometric titrations was performed with factor analysis and with the SPECFIT program.[22b,c] ^1H NMR spectra were recorded at 25 °C on Bruker Avance 400 MHz and Bruker DRX-500 MHz spectrometer. Chemical shifts are given in ppm with respect to TMS. Diffusion ordered spectroscopy (DOSY) was carried out at 500 MHz–Larmor frequency (298 K, 2.5×10^{-3} m, CD_3CN). The used pulse sequence was the Bruker pulse program ledbpgp2s[34] which employs stimulated echo, bipolar gradients and longitudinal eddy current delay as the z filter. The four 2 ms gradient pulses have sine-bell shapes and amplitudes ranging linearly from 2.5 to 50 G cm^{-1} in 32 steps. The diffusion delay was in the range 60–140 ms depending on the analyte diffusion coefficient, and the no. of scans was 32. The processing was done using a line broadening of 5 Hz and the diffusion coefficients were calculated with the Bruker processing package. Pneumatically-assisted electrospray (ESI-MS) mass spectra were recorded from 10^{-4} mol dm^{-3} solutions on Finnigan SSQ7000 and MDS Aciex API III instruments. Elemental analyses were performed by K.-L. Buchwalder from the microchemical Laboratory of the University of Geneva.

Single crystal structure determination of $[Zn_2(L6)Cl](CF_3SO_3)_3 \cdot 2H_2O \cdot 4CH_3CN$ (1)

The crystal was mounted on a quartz fiber with protective oil. Cell dimensions and intensities were measured at 150 K on a Stoe IPDS diffractometer with graphite-monochromated Mo[Kα] radiation (λ = 0.71073 Å). Data were corrected for Lorentz and polarization effects and for absorption. The hydrogen atoms of the methyl groups and of the water molecules were observed and refined with restraints on bond lengths valence angles. All other hydrogen atoms were calculated. As often observed in such large supramolecular crystal structures where the packing is dominated by very large cations with disordered small anions and solvent molecules, the low diffraction pattern led to a poor data to parameters ratio (5.8). One of the triflate anions was disordered and refined on two distinct positions with restraints on bond lengths and bond angles and population parameters of 0.5. All solvent molecules of acetonitrile were refined with restraints on bond lengths and bond angles and showed large atomic displacement parameters. The structure was solved by direct methods (SIR97),[35] all other calculations were performed with XTAL[36] system and ORTEP[37] programs. CCDC-865559 contains all crystallographic data†.

Acknowledgements

Financial support from the Swiss National Science Foundation is gratefully acknowledged. We thank P. Perrottet and E. Sandmeyer for recording ESI-MS spectra and A. Pinto for recording 500 MHz DOSY spectra.

Notes and references

1 (*a*) C. Piguet, G. Bernardinelli, B. Bocquet, A. Quattropanni and A. F. Williams, *J. Am. Chem. Soc.*, 1992, **114**, 7440; (*b*) J.-M. Lehn, *Supramolecular Chemistry – Concepts and Perspectives*, VCH, Weinheim, 1995, ch. 9.

2 (*a*) E. C. Constable and J. V. Walker, *J. Chem. Soc., Chem. Commun.*, 1992, 884; (*b*) E. C. Constable, A. J. Edwards, P. R. Raithby and J. V. Walker, *Angew. Chem., Int. Ed. Engl.*, 1993, **32**, 1465.

3 (*a*) V. C. Smith and J.-M. Lehn, *Chem. Commun.*, 1996, 2733; (*b*) A. Marquis, V. Smith, J. M. Harrowfield, J.-M. Lehn, H. Herschbach, R. Sanvito, E. Leize-Wagner and A. van Dorsselaer, *Chem.–Eur. J.*, 2006, **12**, 5632.

4 C. Piguet, B. Bocquet and G. Hopfgartner, *Helv. Chim. Acta*, 1994, **77**, 931.

5 C. Piguet, G. Hopfgartner, B. Bocquet, O. Schaad and A. F. Williams, *J. Am. Chem. Soc.*, 1994, **116**, 9092.

6 C. Piguet, G. Bernardinelli, A. F. Williams and B. Bocquet, *Angew. Chem., Int. Ed. Engl.*, 1995, **34**, 582.

7 C. Piguet, *J. Inclusion Phenom. Macrocyclic Chem.*, 1999, **34**, 361.

8 (*a*) C. Dietrich-Buchecker, N. Geum, A. Hori, M. Fujita, S. Sakamoto, K. Yamaguchi and J.-P. Sauvage, *Chem. Commun.*, 2001, 1182; (*b*) C. Dietrich-Buchecker, B. Colasson, M. Fujita, A. Hori, N. Geum, S. Sakamoto, K. Yamaguchi and J.-P. Sauvage, *J. Am. Chem. Soc.*, 2003, **125**, 5717.

9 (*a*) D. J. Cardenas, P. Gavina and J.-P. Sauvage, *J. Am. Chem. Soc.*, 1997, **119**, 2656; (*b*) D. J. Cardenas and J.-P. Sauvage, *Inorg. Chem.*, 1997, **36**, 2777.

10 S. P. Argent, H. Adams, L. P. Harding, T. Riis-Johannessen, J. C. Jeffery and M. D. Ward, *New J. Chem.*, 2005, **29**, 904.

11 S. P. Argent, H. Adams, T. Riis-Johannessen, J. C. Jeffery, L. P. Harding, W. Clegg, R. W. Harrington and M. D. Ward, *Dalton Trans.*, 2006, 4996.

12 (*a*) G. Ercolani, *J. Am. Chem. Soc.*, 2003, **125**, 16097; (*b*) C. Piguet, M. Borkovec, J. Hamacek and K. Zeckert, *Coord. Chem. Rev.*, 2005, **249**, 705; (*c*) J. Hamacek, M. Borkovec and C. Piguet, *Dalton Trans.*, 2006, 1473; (*d*) C. Piguet, *Chem. Commun.*, 2010, **46**, 6209; (*e*) G. Ercolani and L. Schiaffino, *Angew. Chem., Int. Ed.*, 2011, **50**, 1762.

13 (*a*) G. Schwarzenbach, *Helv. Chim. Acta*, 1952, **35**, 2344; (*b*) A. W. Adamson, *J. Am. Chem. Soc.*, 1954, **76**, 1578; (*c*) A. E. Martell, *Adv. Chem.*, 1966, **62**, 272; (*d*) D. Munro, *Chem. Br.*, 1977, **13**, 100; (*e*) E. L. Simmons, *J. Chem. Educ.*, 1979, **56**, 578; (*f*) C.-S. Chung, *J. Chem. Educ.*, 1984, **61**, 1062.

14 (*a*) S. W. Benson, *J. Am. Chem. Soc.*, 1958, **80**, 5151; (*b*) W. F. Bailey and A. S. Monahan, *J. Chem. Educ.*, 1978, **55**, 489; (*c*) G. Ercolani, C. Piguet, M. Borkovec and J. Hamacek, *J. Phys. Chem. B*, 2007, **111**, 12195.

15 (*a*) G. Koper and M. Borkovec, *J. Phys. Chem. B*, 2001, **105**, 6666; (*b*) M. Borkovec, G. J. M. Koper and C. Piguet, *Curr. Opin. Colloid Interface Sci.*, 2006, **11**, 280; (*c*) G. J. M. Koper and M. Borkovec, *Polymer*, 2010, **51**, 5649.

16 For simplification purposes, each bidentate or tridentate binding unit is considered as a single point connector for the entering metal.

17 (*a*) G. Ercolani, L. Mandolini, P. Mencarelli and S. Roelens, *J. Am. Chem. Soc.*, 1993, **115**, 3901; (*b*) P. I. Kitov and D. R. Bundle, *J. Am. Chem. Soc.*, 2003, **125**, 16271; (*c*) A. Mulder, J. Huskens and D. N. Reinhoudt, *Org. Biomol. Chem.*, 2004, **2**, 3409; (*d*) D. H. Williams, E. Stephens, D. P. O'Brien and M. Zhou, *Angew. Chem., Int. Ed.*, 2004, **43**, 6596; (*e*) J. D. Badjic, A. Nelson, S. J. Cantrill, W. B. Turnbull and J. F. Stoddart, *Acc. Chem. Res.*, 2005, **38**, 723; (*f*) H.-J. Schneider and A. K. Yatsimirsky, *Chem. Soc. Rev.*, 2008, **37**, 263; (*g*) T. Rehm and C. Schmuck, *Chem. Commun.*, 2008, 801.

18 (*a*) W. Kuhn, *Kolloid-Z.*, 1934, **68**, 2; (*b*) H. Jacobson and W. H. Stockmayer, *J. Chem. Phys.*, 1950, **18**, 1600; (*c*) P. J. Flory, U. W. Suter and M. Mutter, *J. Am. Chem. Soc.*, 1976, **98**, 5733; (*d*) W. P. Jencks, *Proc. Natl. Acad. Sci. U. S. A.*, 1981, **78**, 4046; (*e*) M. A. Winnik, *Chem. Rev.*, 1981, **81**, 491; (*f*) X. Chi, A. J. Guerin, R. A. Haycock, C. A. Hunter and L. D. Sarson, *J. Chem. Soc., Chem. Commun.*, 1995, 2563; (*g*) G. Ercolani, *J. Phys. Chem. B*, 1998, **102**, 5699; (*h*) R. H. Kramer and J. W. Karpen, *Nature*, 1998, **395**, 710; (*i*) C. Galli and L. Mandolini, *Eur. J. Org. Chem.*, 2000, 3117; (*j*) J. M. Gargano, T. Ngo, J. Y. Kim, D. W. K. Acheson and W. J. Lees, *J. Am. Chem. Soc.*, 2001, **123**, 12909.

19 (*a*) N. Dalla Favera, J. Hamacek, M. Borkovec, D. Jeannerat, F. Gumy, J.-C. G. Bünzli, G. Ercolani and C. Piguet, *Chem.–Eur. J.*, 2008, **14**, 2994; (*b*) T. Riis-Johannessen, N. Dalla Favera, T. K. Todorova, S. M. Huber, L. Gagliardi and C. Piguet, *Chem.–Eur. J.*, 2009, **15**, 12702.

20 N. Dalla Favera, U. Kiehne, J. Bunzen, S. Hyteballe, A. Lützen and C. Piguet, *Angew. Chem., Int. Ed.*, 2010, **49**, 125.

21 T. Riis-Johannessen, G. Bernardinelli, Y. Filinchuk, S. Clifford, N. Dalla Favera and C. Piguet, *Inorg. Chem.*, 2009, **48**, 5512.

22 (*a*) E. R. Malinowski and D. G. Howery, *Factor Analysis in Chemistry*, Wiley, New York, Chichester, 1980; (*b*) H. Gampp, M. Maeder, C. J. Meyer and A. D. Zuberbühler, *Talanta*, 1985, **23**, 1133; (*c*) H. Gampp, M. Maeder, C. J. Meyer and A. D. Zuberbühler, *Talanta*, 1986, **33**, 943.

23 A. Escande, L. Guénée, K.-L. Buchwalder and C. Piguet, *Inorg. Chem.*, 2009, **48**, 1132.

24 M. Cantuel, F. Gumy, J.-C. G. Bünzli and C. Piguet, *Dalton Trans.*, 2006, 2647.

25 S. Petoud, J.-C. G. Bünzli, F. Renaud, C. Piguet, K. J. Schenk and G. Hopfgartner, *Inorg. Chem.*, 1997, **36**, 5750.

26 G. A. Orpen, L. Brammer, F. H. Allen, O. Kennard, D. G. Watson and R. Taylor, *J. Chem. Soc., Dalton Trans.*, 1989, S1.

27 R. D. Shannon, *Acta Crystallogr., Sect. A: Cryst. Phys., Diffr., Theor. Gen. Crystallogr.*, 1976, **32**, 751.

28 J.-M. Lehn and A. V. Eliseev, *Science*, 2001, **291**, 2331.

29 For the sake of clarity, counter-anions and solvent molecules are omitted in equilibrium (9). Although $[Zn_3(\mathbf{L6})_2]^{6+}$ can be detected only as a minor species by ESI-MS, its ^{1}H NMR signature at 5.88 ppm combined with the exclusive isolation of macrocyclic complexes and [2]catenates with ligand **L5** and **L6** justify its consideration into eqn (9) instead of $[Zn_2(\mathbf{L6})_2]^{4+}$ preferably detected in the gas phase. We suspect that the constrained $[Zn_3(\mathbf{L6})_2]^{6+}$ catenate transforms into $[Zn_2(\mathbf{L6})_2]^{4+}$ upon electrospray ionization followed by desolvation accompanying the transfer in the gas phase.

30 The third powers of the ratios $(D_{ZnL2}/D_{Zn2L})^3 = 0.66(7)$ and $(D_{Zn3L2}/D_{Zn2L})^3 = 0.60(6)$ compare well with the ratios of the molecular weights $MM_{Zn2L}/MM_{ZnL2} = 0.67$ and $MM_{Zn2L}/MM_{Zn3L2} = 0.62$, a mathematical relationship predicted for large free diffusing pseudo-spherical molecules in an ideal solvent, see A. Macchioni, G. Ciancaleoni, C. Zuccaccia and D. Zuccaccia, *Chem. Soc. Rev.*, 2008, **37**, 479.

31 J.-F. Lemonnier, L. Guénée, G. Bernardinelli, J.-F. Vigier, B. Bocquet and C. Piguet, *Inorg. Chem.*, 2010, **49**, 1252.

32 J. F. Desreux, in *Lanthanide Probes in Life, Chemical and Earth Sciences*, ed. J.-C. G. Bünzli and G. R. Choppin, Elsevier, Amsterdam, 1989, ch. 2, p. 43.

33 G. Schwarzenbach, *Complexometric Titrations*, Chapman & Hall, London, 1957, p. 8.

34 D. Wu, A. Chen and C. S. Johnson Jr, *J. Magn. Reson., Ser. A*, 1995, **115**, 260.

35 A. Altomare, M. C. Burla, M. Camalli, G. Cascarano, C. Giacovazzo, A. Guagliardi, G. Moliterni, G. Polidori and R. Spagna, *J. Appl. Crystallogr.*, 1999, **32**, 115.

36 *XTAL 3.2 User's Manual*, ed. S. R. Hall, H. D. Flack and J. M. Stewart, Universities of Western Australia and Maryland, 1989.

37 C. K. Johnson, ORTEP II; Report ORNL-5138, Oak Ridge National Laboratory, Oak Ridge, Tennessee, 1976.

Electronic Supplementary Material (ESI) for Dalton Transactions

Looking for the origin of the switch between coordination-captured helicates and catenates.

Lilit Aboshyan-Sorgho, Martine Cantuel, Gérald Bernardinelli, and Claude Piguet*

Supporting Information (13 pages)

Table S1 Summary of crystal data, intensity measurement and structure refinement for $[Zn_2(\mathbf{L6})Cl](CF_3SO_3)_3(H_2O)_2(CH_3CN)_4$ (**1**).

Compound	**1**
Formula	$Zn_2C_{62}H_{59}N_{15}Cl_1O_{11}F_9S_3$
fw	1623.7
Crystal system	triclinic
Space Group	$P\bar{1}$
a (Å)	12.4234(8)
b (Å)	17.5344(12)
c (Å)	18.8655(13)
α (deg)	68.137(8)
β (deg)	71.102(7)
γ (deg)	73.688(8)
V (Å^3)	3547.8(5)
Z	2
Crystal Size (mm)	0.054 x 0.13 x 0.25
d_{calcd} (Mg m^{-3})	1.520
μ(MoKα) (mm^{-1})	0.894
*T*min, *T*max	0.8203 , 0.9495
2θmax (deg)	51.2
No. of reflns collected	26547
No. of independent reflns	12893
No. of obsd [a] (used[b]) reflns	5709 (5816)
No. of variables	1000
Weighting scheme *p* [c]	0.00025
Max and min $\Delta\rho$ (e Å^{-3})	1.15 , -1.02
GOF (*F*) [d] (all data)	1.01(1)
R [e], ωR [f]	0.051 , 0.046

[a] $|Fo| > 4\sigma(Fo)$; [b] Used in the refinements (including reflns with $|Fo| \le 4\sigma(Fo)$ if $|Fc| > |Fo|$); [c] $\omega = 1/[\sigma^2 (F_o) + p (F_o)^2]$; [d] $S = [\Sigma \{((F_o-F_c) / \sigma(F_o))^2 \} / (N_{ref} - N_{var})]^{1/2}$; [e] $R = \Sigma ||F_o| - |F_c|| / \Sigma |F_o|$; [f] $\omega R = [\Sigma (\omega|Fo|-|Fc|)^2 / \Sigma \omega|Fo|^2]^{1/2}$.

Table S2 Distances and angles between H-bond donors and acceptors in the crystal structure of $[Zn_2(\mathbf{L6})(Cl)(H_2O)_2(CF_3SO_3)](CF_3SO_3)_2(CH_3CN)_4$ (**1**). (numbering scheme is given in Fig. 6 and a pictorial illustration in Fig. S5).

D-H···A	*d* (D-H)/ Å	*d* (H···A)/ Å	d (D···A)/ Å	∠ (D-H···A)/ °
O(1w)-H(11w)···O(1b)	0.96	1.77	2.692(8)	160
O(1w)-H(12w)···O(3a)	0.98	1.68	2.640(7)	164
O(2w)-H(21w)···Cl(1)	0.98	2.17	3.115(5)	163
O(2w)-H(22w)···O(2c)	0.97	1.70	2.66(3)	170

Table S3 Bond distances [Å] and bond angles [°] in the molecular structure of the cation $[Zn_2(\mathbf{L6})(Cl)(H_2O)_2(CF_3SO_3)]^{2+}$ (numbering scheme is given in Fig. 6).

Bond distances / Å

Zn1-N1	2.113(6)	Zn1-N2	2.131(5)
Zn1-N7	2.137(6)	Zn1-Cl1	2.252(3)
Zn1-O1w	2.004(6)		
Zn2-N4	2.087(5)	Zn2-N6	2.144(6)
Zn2-N9	2.077(6)	Zn2-N11	2.157(9)
Zn2-O2w	2.067(5)	Zn2-O1a	2.340(7)

Bond Angles / °

N1-Zn1-N2	75.1(2)	N2-Zn1-N7	150.2(3)
N1-Zn1-N7	75.2(2)	N2-Zn1-O1w	92.1(3)
N1-Zn1-O1w	107.7(3)	N2-Zn1-Cl1	100.7(2)
N1-Zn1-Cl1	133.9(2)	N7-Zn1-O1w	99.0(3)
O1w-Zn1-Cl1	118.4(2)	N7-Zn1-Cl1	98.1(2)
N4-Zn2-N6	78.4(2)	N6-Zn2-N9	94.9(3)
N4-Zn2-N9	171.8(2)	N6-Zn2-N11	98.1(3)
N4-Zn2-N11	98.7(3)	N6-Zn2-O1a	86.4(3)
N4-Zn2-O1a	89.7(3)	N6-Zn2-O2w	166.3(3)
N4-Zn2-O2w	94.4(2)	N9-Zn2-N11	77.5(3)
N11-Zn2-O1a	171.1(2)	N9-Zn2-O1a	94.6(3)
N11-Zn2-O2w	94.5(2)	N9-Zn2-O2w	93.1(2)
O1a-Zn2-O2w	81.9(3)		

Table S4 Selected Least-Squares Planes Data for **1**.

Least-squares planes description	Abbreviation	Max. deviation/Å	Atom
Pyridine, N1	py1	0.005	C5
Benzimidazole, N2, N3	bz1a	0.008	C6
Benzimidazole, N4, N5	bz2a	0.017	C19
Pyridine, N6	py2a	0.023	C24
Benzimidazole, N7, N8	bz1b	0.010	C29
Benzimidazole, N9, N10	bz2b	0.016	C34
Pyridine, N11	py2b	0.013	C42

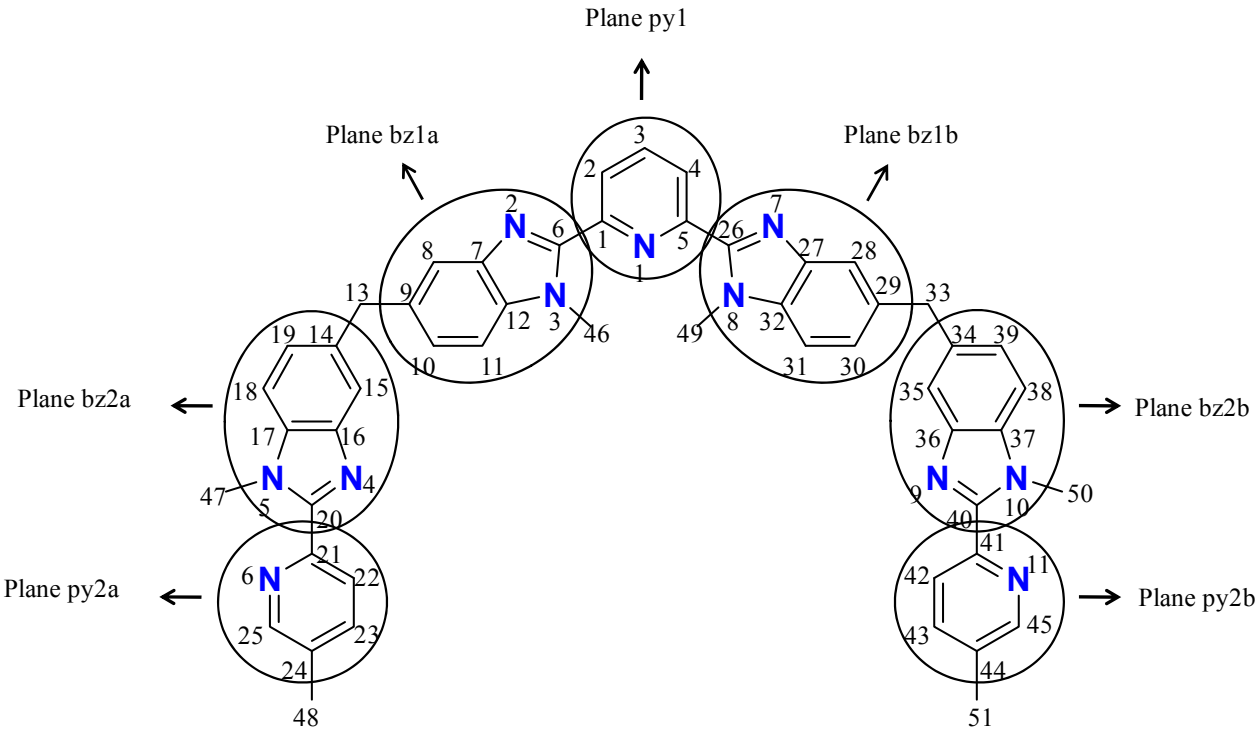

Intramolecular interplanar angles /°

	py1	bz1a	bz2a	py2a	bz1b	bz2b
bz1a	4.6(2)					
bz2a	65.3(2)	65.9(2)				
py2a	48.9(2)	50.4(2)	18.5(2)			
bz1b	7.6(2)	9.6(2)	57.7(2)	41.4(2)		
bz2b	56.2(2)	51.8(2)	84.9(1)	90.0(2)	60.1(2)	
py2b	52.4(3)	48.4(2)	80.7(2)	88.4(2)	57.4(2)	9.1(2)

Intermolecular interplanar distances and angles involved in stacking interactions (°)

Plane 1 - plane 2#	Symmetry operation for plane 2#	$\bar{d}$ /Å	∠ (plane 1, plane 2#) /°
py1 - bz1a #	(1-x, 1-y, 1-z)	3.52(8)	4.6(2)
bz2a – bz2a #	(1-x, 2-y, -z)	3.413(10)	0
bz1b - bz1b #	(-x, 1-y, 1-z)	3.717(6)	0
bz2b – bz2b #	(-x, 2-y, 1-z)	3.308(8)	0

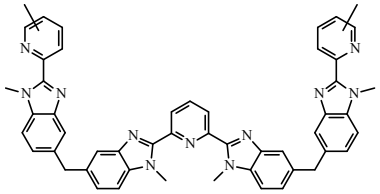

$$2\,\mathbf{L}\boldsymbol{k} + [Fe(CH_3CN)_6]^{2+} + 2\,[Ag(CH_3CN)_4]^{+} \underset{}{\overset{\beta_{1,2,2}^{Fe,Ag,\mathbf{L}\boldsymbol{k}}}{\rightleftharpoons}} [FeAg_2(\mathbf{L}\boldsymbol{k})_2]^{4+} + 14\,CH_3CN \quad (3)$$

				helicate	catenate		
					PP/*MM*	*MP*	
Point groups:	C_{2v}	O_h	T_d	D_2	D_2	S_4	C_{3v}
σ^{ext}:	2	24	12	4	4	2	3
σ^{int}:	3^6	3^6	3^4	3^{12}	3^{12}	3^{12}	1
σ^{chiral}:	1	1	1	1/2	1/2	1	1

$$\omega_{1,2,2}^{Fe,Ag,\mathbf{L}\boldsymbol{k}}(D_2) = \frac{\left(2\cdot 3^6\right)^2\left(24\cdot 3^6\right)\left(12\cdot 3^4\right)^2}{\left(4\cdot 3^{12}\right)3^{14}} = 3456 \qquad \omega_{1,2,2}^{chiral}(D_2) = \frac{1^2\cdot 1\cdot 1^2}{(1/2)\cdot 1^{14}} = 2$$

$$\Rightarrow \omega_{1,2,2}^{Fe,Ag,\mathbf{L}\boldsymbol{k}}\omega_{1,2,2}^{chiral}(D_2) = 3456\cdot 2 = 6912$$

$$\omega_{1,2,2}^{Fe,Ag,\mathbf{L}\boldsymbol{k}}(S_4) = \frac{\left(2\cdot 3^6\right)^2\left(24\cdot 3^6\right)\left(12\cdot 3^4\right)^2}{\left(2\cdot 3^{12}\right)3^{14}} = 6912 \qquad \omega_{1,2,2}^{chiral}(S_4) = \frac{1^2\cdot 1\cdot 1^2}{1\cdot 1^{14}} = 1$$

$$\Rightarrow \omega_{1,2,2}^{Fe,Ag,\mathbf{L}\boldsymbol{k}}\omega_{1,2,2}^{chiral}(S_4) = 6912\cdot 1 = 6912$$

Figure S1 Symmetry numbers (σ) and statistical factors (ω) for the complexation of $[Fe(CH_3CN)_6]^{2+}$ and $[Ag(CH_3CN)_4]^{+}$ to **L5** or **L6** in acetonitrile. The two diastereomeric [2]catenates with D_2 (*PP*/*MM* enantiomers) and S_4 (meso-*PM* isomer) symmetries are considered.

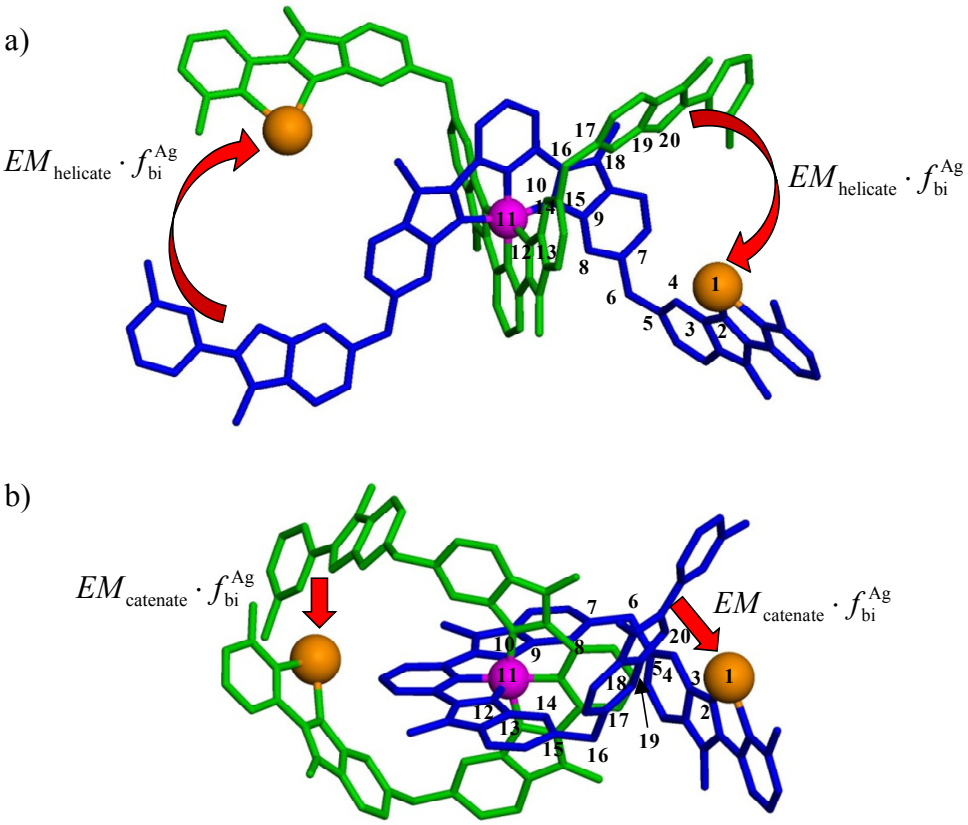

Figure S2 Schematic illustration of the intramolecular macrocyclization processes responsible for the formation of $[AgFeAg(\mathbf{L5})_2]^{4+}$ as a) a double-stranded helicate and b) a [2]catenate. The twenty atoms of the crooked chains connecting the interacting groups are highlighted.

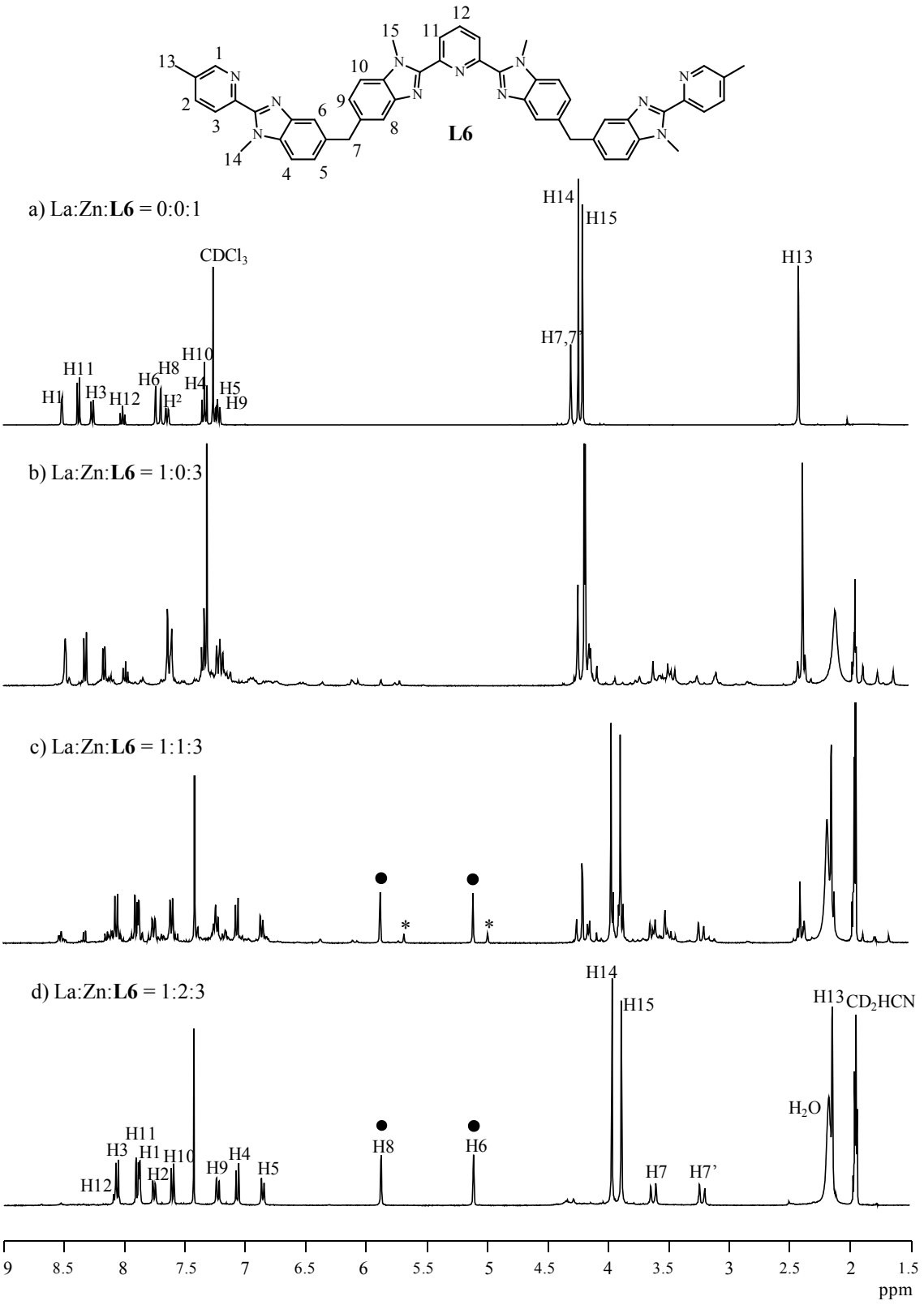

Figure S3 ^{1}H NMR titration of **L6** (10^{-2} M) with La(III) and Zn(II) in $CDCl_3/CD_3CN$ = 1:1 at 293 K with numbering scheme and highlighting the chemical shifts for H6 and H8 during the successive formation of $[LaZn(\mathbf{L6})_3]^{5+}$ (*) and $[ZnLaZn(\mathbf{L6})_3]^{7+}$ (•) . Adapted from ref. 24.

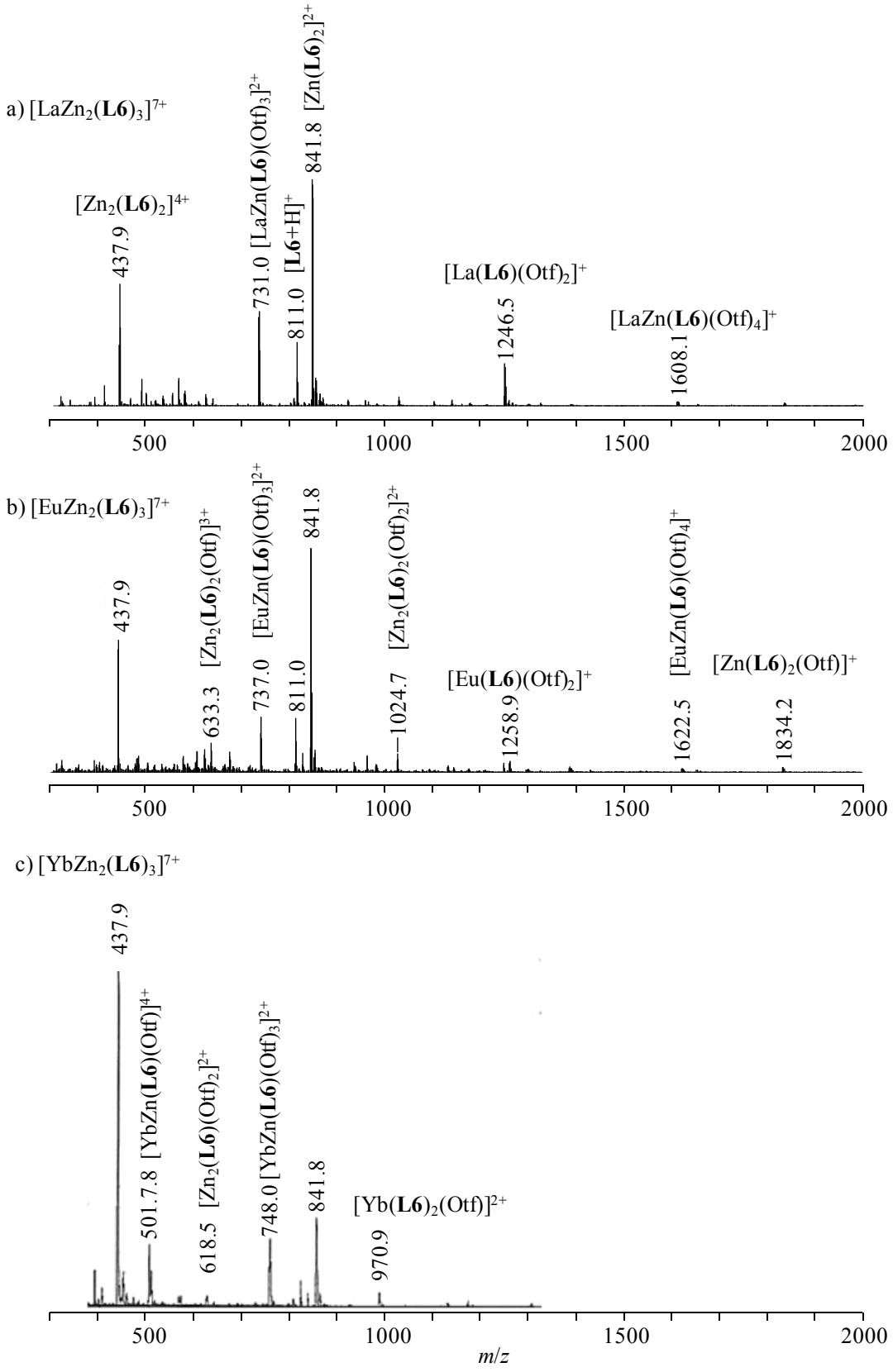

Figure S4 ESI-MS spectra of $[LnZn_2(\mathbf{L6})_3]^{7+}$ with a) Ln = La (10^{-4} M), b) Ln = Eu (10^{-4} M) and c) Ln = Yb ($5 \cdot 10^{-4}$ M) in CH_3CN:$CHCl_3$ (1:1) at 298 K ($Otf^- = CF_3SO_3^-$).

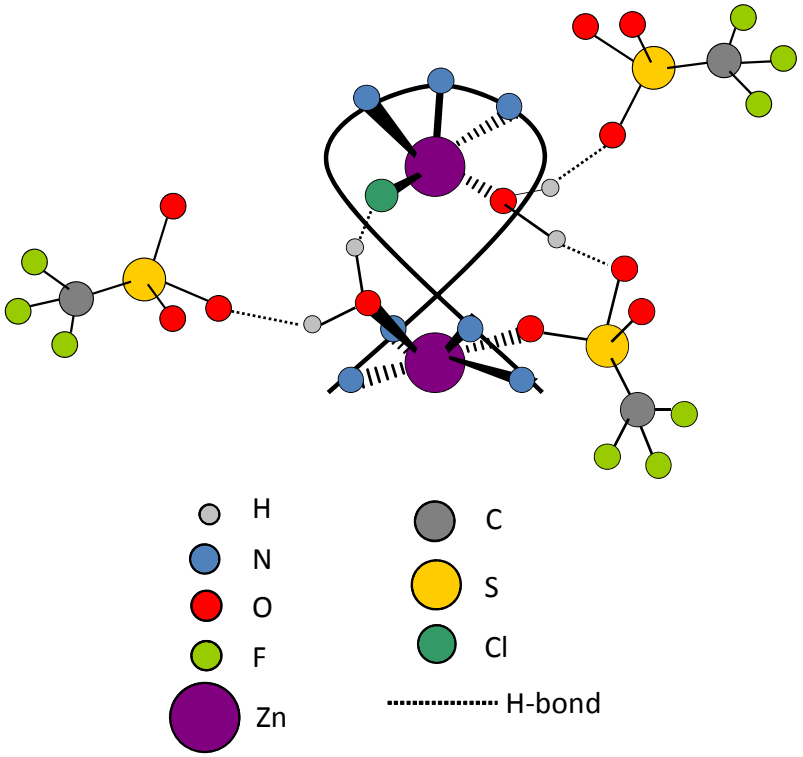

Figure S5 Schematic view of the hydrogen bonding network in the crystal structure of $[Zn_2(\mathbf{L6})(Cl)(H_2O)_2(CF_3SO_3)](CF_3SO_3)_2(CH_3CN)_4$ (**1**). The acetonitrile molecules are not involved in hydrogen bonding and are thus omitted for clarity.

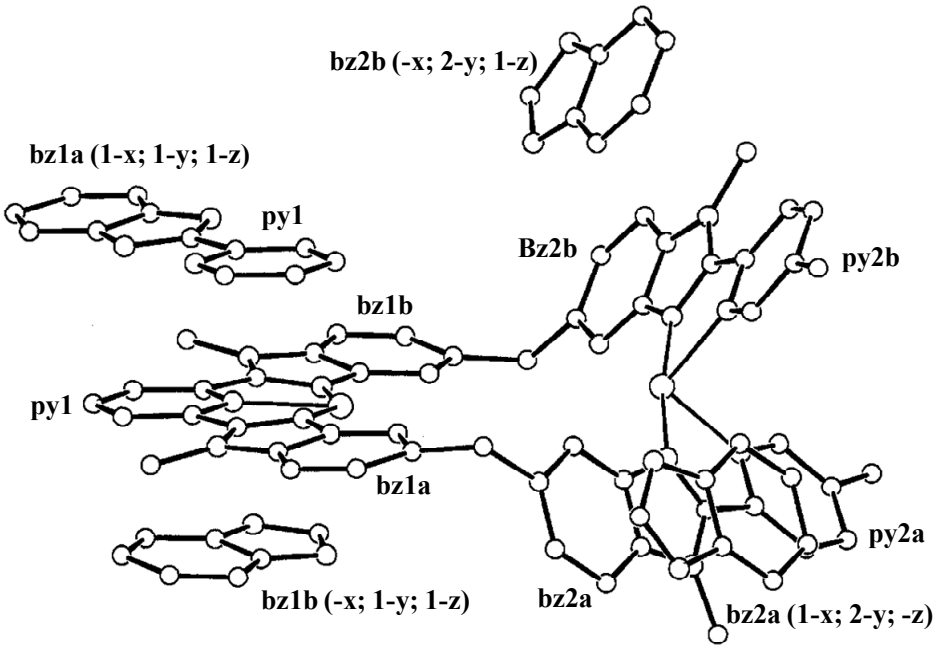

Figure S6 Aromatic rings involved in intermolecular π-stacking interactions in the crystal structure of $[Zn_2(\mathbf{L6})(Cl)(H_2O)_2(CF_3SO_3)](CF_3SO_3)_2(CH_3CN)_4$ (**1**). The symmetry operations relating the various molecules are given between parentheses. Interplanar angles and distances are collected in Table S4.

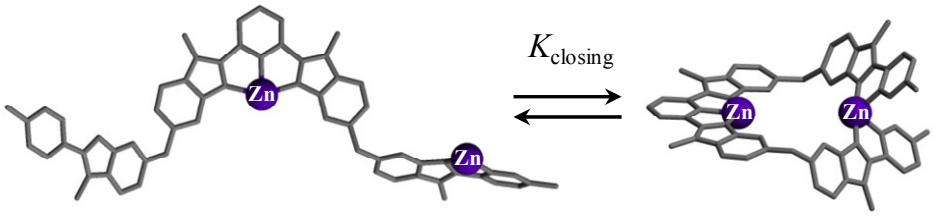

(7)

Acyclic-$[Zn_2(\mathbf{L6})]^{4+}$ cyclic-$[Zn_2(\mathbf{L6})]^{4+}$

Point groups:	C_s	C_2
σ^{ext}:	1	2
σ^{int}:	3^6	3^6
σ^{chiral}:	1	1/2

$$\omega_{closing}^{geometry} = \frac{\left(1 \cdot 3^6\right)}{\left(2 \cdot 3^6\right)} = 1/2 \qquad \omega_{closing}^{chiral} = \frac{1}{(1/2)} = 2$$

$$\Rightarrow \omega_{closing} = \omega_{closing}^{geometry} \cdot \omega_{closing}^{chiral} = \frac{1}{2} \cdot 2 = 1$$

Figure S7 Symmetry numbers (σ) and statistical factors (ω) for the macrocyclization of $[Zn_2(\mathbf{L6})]^{4+}$ in acetonitrile.

Appendix 1. Experimental speciation obtained by ^{1}H NMR for equilibrium 9.

For a given stoichiometric $|Zn|_{tot} / |\mathbf{L6}|_{tot}$ ratio, the integrated intensities of the ^{1}H NMR signals recorded for the same proton in $[Zn_2(\mathbf{L6})]^{4+}$ (I_{Zn2L}), $[Zn(\mathbf{L6})_2]^{2+}$ (I_{ZnL2}) and $[Zn_3(\mathbf{L6})_2]^{6+}$ (I_{Zn3L2}) can be compared according to equilibrium 9 (eq. S1) and scaled with respect to $|Zn_2(\mathbf{L6})|$ (eq. S2).

$$\frac{|Zn(\mathbf{L6})_2|}{|Zn_3(\mathbf{L6})_2|} = \left(\frac{I_{ZnL2}}{I_{Zn3L2}}\right) = 1 \qquad \text{(S1)}$$

$$\frac{|Zn(\mathbf{L6})_2|}{|Zn_2(\mathbf{L6})|} = \left(\frac{I_{ZnL2}}{2I_{Zn2L}}\right) \qquad \text{(S2)}$$

Introducing eqs (S1) and (S2) into the mass balance eq. (S3) yields eq. (S4) after straightforward algebraic transformations.

$$|\mathbf{L6}|_{tot} = |Zn_2(\mathbf{L6})| + 2|Zn(\mathbf{L6})_2| + 2|Zn_3(\mathbf{L6})_2| \qquad \text{(S3)}$$

$$|Zn_2(\mathbf{L6})| = |\mathbf{L6}|_{tot}\left(\frac{I_{Zn2L}}{I_{Zn2L} + 2I_{ZnL2}}\right) \qquad \text{(S4)}$$

Introducing eq. (S4) into eqs (S1) and (S2) gives the remaining complex speciation

$$|Zn(\mathbf{L6})_2| = |Zn_3(\mathbf{L6})_2| = |\mathbf{L6}|_{tot}\left(\frac{I_{ZnL2}}{2\left(I_{Zn2L} + 2I_{ZnL2}\right)}\right) \qquad \text{(S5)}$$

The missing concentration $|Zn|$ shown in eq. (S7) can be deduced from the mass balance written for the metal concentration (eq. S6).

$$|Zn| = |Zn|_{tot} - |Zn(\mathbf{L6})_2| - 2|Zn_2(\mathbf{L6})| - 3|Zn_3(\mathbf{L6})_2| \qquad \text{(S6)}$$

$$|Zn| = |Zn|_{tot} - 2|\mathbf{L6}|_{tot}\left(\frac{I_{Zn2L} + I_{ZnL2}}{I_{Zn2L} + 2I_{ZnL2}}\right) \qquad \text{(S7)}$$

The final introduction of the various concentrations expressed in eqs (S4)-(S7) into the law of mass action associated with equilibrium (9) yields eq. (S8) for $|Zn|_{tot} = 2|\mathbf{L6}|_{tot}$ (the standard concentration of the reference state is set at c^{θ} =1 M).

$$K_{exch} = \frac{|Zn(\mathbf{L6})_2| \cdot |Zn_3(\mathbf{L6})_2| \cdot |Zn|^4}{|Zn_2(\mathbf{L6})|^4} = 4\left(|\mathbf{L6}|_{tot}\right)^2 \frac{\left(I_{ZnL2}\right)^6}{\left(I_{Zn2L}\right)^4\left(I_{Zn2L} + 2I_{ZnL2}\right)^2} \qquad \text{(S8)}$$

Integration of the signals for H8 in the ^{1}H NMR spectrum of $[Zn_2(\mathbf{L6})Cl(CF_3SO_3)(H_2O)_2](CF_3SO_3)_2$ ($|\mathbf{L6}|_{tot}$ = 2.5 mM, CD_3CN, 293 K, Fig. 9) gave I_{Zn2L} = 5 and I_{ZnL2} = 1, from which we calculated $|Zn_2(\mathbf{L6})|$ = $1.79\cdot10^{-3}$ M (eq S4), $|Zn(\mathbf{L6})_2| = |Zn_3(\mathbf{L6})_2|$ = $1.79\cdot10^{-4}$ M (eq. S5), $|Zn|$ = $7.14\cdot10^{-4}$ M (eq. S7) and K_{exch} = $8.16\cdot10^{-10}$.

Appendix 2. **Thermodynamic model for equilibrium 9**.

$$4\,[Zn_2(\mathbf{L6})]^{4+} \underset{}{\overset{K_{exch}}{\rightleftharpoons}} [Zn(\mathbf{L6})_2]^{2+} + [Zn_3(\mathbf{L6})_2]^{6+} + 4\,[Zn]^{2+} \quad (9)$$

Point groups:	C_2	D_{2d}	S_4	O_h
σ^{ext}:	2	4	2	24
σ^{int}:	3^6	3^{12}	3^{12}	1
σ^{chiral}:	1/2	1	1	1

$$\omega_{exch} = \frac{\left(2\cdot 3^6\cdot\left(\tfrac{1}{2}\right)\right)^4}{\left(4\cdot 3^{12}\right)\left(2\cdot 3^{12}\right)(24)^4} = \frac{1}{2654208}$$

$$\Rightarrow K_{exch} = \omega_{exch}\frac{\left[\left(f_{tri}^{Zn}\right)^2 u_{tri}^{\mathbf{L6},\mathbf{L6}}\right]\cdot\left[\left(f_{tri}^{Zn}\right)^2\left(f_{bi}^{Zn}\right)^4\left(EM_{catenate}\right)^2 u_{tri}^{\mathbf{L6},\mathbf{L6}}\left(u_{bi}^{\mathbf{L6},\mathbf{L6}}\right)^2\left(u^{Zn,Zn}\right)^2\right]}{\left[\left(f_{tri}^{Zn}\right)\left(f_{bi}^{Zn}\right)^2\left(EM_{catenate}\right)\left(u_{bi}^{\mathbf{L6},\mathbf{L6}}\right)\left(u^{Zn,Zn}\right)\right]^4}$$

$$\Rightarrow K_{exch} = \omega_{exch}\left(\frac{u_{tri}^{\mathbf{L6},\mathbf{L6}}}{u_{bi}^{\mathbf{L6},\mathbf{L6}}}\frac{1}{EM_{catenate}\cdot\left(f_{bi}^{Zn}\right)^2\cdot u^{Zn,Zn}}\right)^2 \quad (10)$$